ARTICLES
PUBLISHED ONLINE: 23 JANUARY 2017 | DOI: 10.1038/NCLIMATE3204
nature climate change

Accelerating net terrestrial carbon uptake during the warming hiatus due to reduced respiration

Ashley Ballantyne[1]*, William Smith[2], William Anderegg[3], Pekka Kauppi[4], Jorge Sarmiento[5], Pieter Tans[6], Elena Shevliakova[7], Yude Pan[8], Benjamin Poulter[9], Alessandro Anav[10], Pierre Friedlingstein[10], Richard Houghton[11] and Steven Running[1]

The recent 'warming hiatus' presents an excellent opportunity to investigate climate sensitivity of carbon cycle processes. Here we combine satellite and atmospheric observations to show that the rate of net biome productivity (NBP) has significantly accelerated from −0.007 ± 0.065 PgC yr^{-2} over the warming period (1982 to 1998) to 0.119 ± 0.071 PgC yr^{-2} over the warming hiatus (1998–2012). This acceleration in NBP is not due to increased primary productivity, but rather reduced respiration that is correlated (r = 0.58; P = 0.0007) and sensitive (γ = 4.05 to 9.40 PgC yr^{-1} per °C) to land temperatures. Global land models do not fully capture this apparent reduced respiration over the warming hiatus; however, an empirical model including soil temperature and moisture observations better captures the reduced respiration.

The terrestrial biosphere removes approximately one-quarter of anthropogenic carbon (C) emissions from the atmosphere[1]; however, considerable uncertainty in climate predictions is due to poorly constrained terrestrial carbon cycle processes that may lead to positive or negative carbon–climate feedbacks[2]. Observations suggest that much of the variability in the global C cycle arises from the terrestrial biosphere response to tropical climate variability[3–6]. However, attributing this response to specific terrestrial processes remains challenging because increased tropical temperatures can suppress primary productivity[7] and/or promote respiration[8], both of which reduce net terrestrial C uptake. Biases have also been identified in the C cycle of Earth System Models (ESMs) that may compromise their climate predictions[5,9,10], but diagnosing the specific C cycle processes contributing to these biases is exceedingly difficult. Thus, disentangling the climate sensitivity of terrestrial productivity and respiration is imperative for advancing our knowledge of global C cycle processes and their potential feedbacks on future climate predictions[2].

We combine atmospheric CO_2 measurements with satellite observations in a complementary way to isolate the main terrestrial C cycle processes:

$$\mathrm{NBP} = \mathrm{GPP} - \mathrm{TER} \quad (1)$$

Net biome productivity (NBP) is estimated as the residual terrestrial carbon sink from atmospheric CO_2 measurements, while accounting for emissions from fossil fuels and land use, and accounting for ocean C uptake. Gross primary productivity (GPP) is approximated from satellite observations[10] and total ecosystem respiration (TER) is calculated as the difference, that is, GPP–NBP, with each term being a positive number. Although there are numerous C loss pathways from ecosystems[11,12], the sum of autotrophic respiration by plants, and heterotrophic respiration by microbes (that is, TER) is the dominant C loss pathway at the global scale. To estimate NBP uncertainty we use a novel 'el camino' approach to simulate the spatial and temporal autocorrelation of errors in atmospheric measurements and emissions, these simulations are then combined to estimate C uptake uncertainty and statistics are performed on all combinations of simulations[13] (see Methods). By separating NBP into its component processes of GPP and TER, we can thus investigate how the climate sensitivity of these processes has changed from the warming period (1982–1998) to the warming hiatus (1998–2012)[14,15].

Has net terrestrial C uptake changed during the warming hiatus? The rate of land surface warming decreased from a significantly increasing trend of 0.031 ± 0.012 °C yr^{-1} (Mann–Kendall, P value = 0.0045) during the warming period to an insignificant trend of 0.009 ± 0.008 °C yr^{-1} (Mann–Kendall, P value = 0.235) during the warming hiatus (Fig. 1a). This decadal change in the rate of land surface warming has been accompanied by an acceleration of NBP from −0.007 ± 0.065 (PgC yr^{-2} (median ± σ) during the warming period to 0.119 ± 0.071 PgC yr^{-2} over the warming hiatus (Fig. 1b). Furthermore, trend analyses that include simulated error estimates show a significant increase in NBP trends during the warming hiatus (two-tailed t-test; t-statistic = 5.39; P value < 0.01; DF = 29), with 54% of the simulated trends in NBP negative during

[1]Department of Ecosystem and Conservation Science, University of Montana, 32 Campus Drive, Missoula, Montana 59801, USA. [2]School of Natural Resources and the Environment, University of Arizona, 1064 East Lowell Street, Tucson, Arizona 85721, USA. [3]Department of Biology, University of Utah, 257 South 1400 East, Room 201, Salt Lake City, Utah 84112-0840, USA. [4]Department of Environmental Science, University of Helsinki, PO Box 65 (Viikinkaari 1), 00014 Helsinki, Finland. [5]Department of Atmospheric and Oceanic Sciences, Princeton University, 300 Forrestal Road, Sayre Hall, Princeton, New Jersey 08544, USA. [6]NOAA ESRL, Global Monitoring Division, 325 Broadway R/GMD, Boulder, Colorado 80305-3328, USA. [7]Geophysical Fluids Dynamics Laboratory, 201 Forrestal Road, Princeton, New Jersey 08540-6649, USA. [8]US Department of Agriculture Forest Service, Newtown Square, Pennsylvania 19073, USA. [9]NASA Goddard Space Flight Center, Greenbelt, Maryland 20771, USA. [10]College of Engineering, Mathematics and Physical Sciences, University of Exeter, North Park Road, Exeter EX4 4QF, UK. [11]Woods Hole Research Center, 149 Woods Hole Road, Falmouth, Massachusetts 02540, USA. *e-mail: ashley.ballantyne@umontana.edu

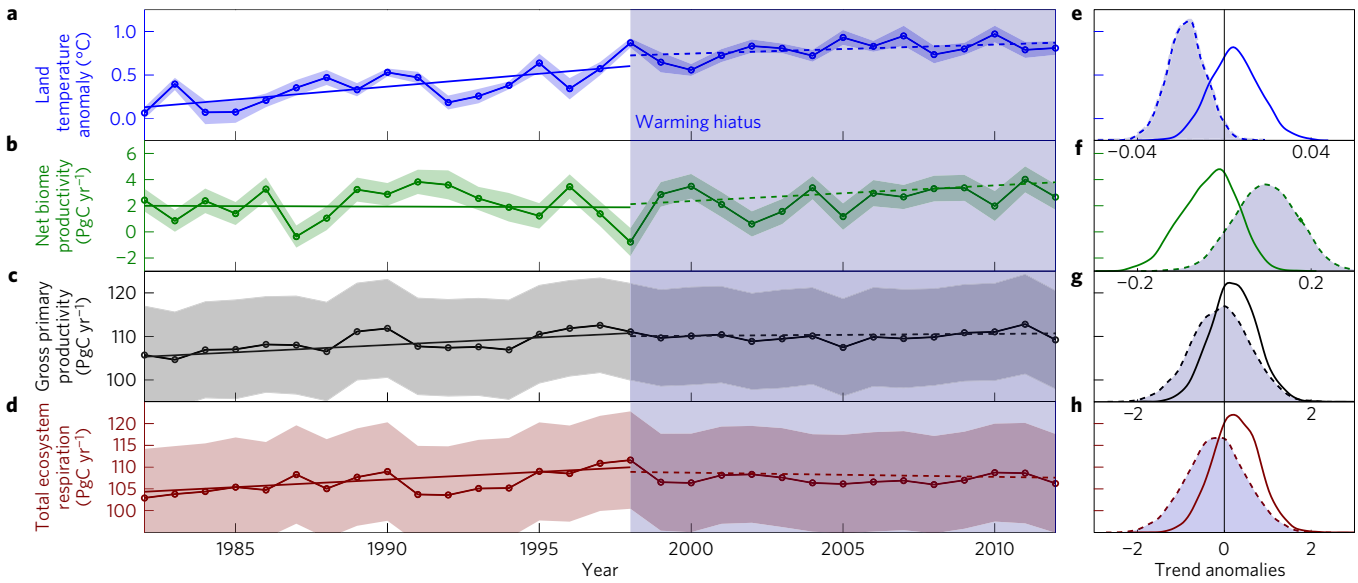

Figure 1 | Changes in trends of land surface temperatures and terrestrial C cycle processes over three decades. a–d, Land surface temperature anomalies[41–43] (**a**), net biome productivity (NBP; **b**)[13], gross primary productivity (GPP; **c**)[44], and total ecosystem respiration (TER ; **d**) are plotted with uncertainty (1σ; shaded areas). Median trend lines from 4,500 simulations are plotted for the warming period from 1982 to 1998 (solid lines) and the warming hiatus (blue window) from 1998 to 2012 (dashed lines). **e–h**, Density functions of trend anomalies normalized to the entire era of common observation are plotted for temperature (**e**), NBP (**f**), GPP (**g**) and TER (**h**), where unfilled densities with solid lines represent trend anomalies over the warming period and grey filled densities with dashed lines represent trend anomalies over the warming hiatus.

the warming period and 96% of the simulated trends in NBP positive during the warming hiatus (Fig. 1f and Table 1). Thus, rates of net terrestrial C uptake have clearly accelerated from the warming period to the warming hiatus.

What terrestrial C cycle processes caused this increase in net terrestrial C uptake during the warming hiatus? The acceleration of NBP can be explained only by an increasing trend in C uptake through GPP and/or a decreasing trend in C loss mainly through TER. Trends in GPP estimated from satellite observations show that GPP has actually levelled from $0.328 \pm 0.602\,\mathrm{PgC\,yr^{-2}}$ during the warming period to $0.042 \pm 0.730\,\mathrm{PgC\,yr^{-2}}$ over the warming hiatus (Fig. 1c). This levelling off of GPP is still evident when meteorological variables required to calculate GPP are held constant or independent estimates of global GPP up-scaled from flux towers are considered (Supplementary Fig. 3). Total respiration rates appear to have decreased from $0.335 \pm 0.605\,\mathrm{PgC\,yr^{-2}}$ during the warming period, with 72% of the simulated trends positive, to $-0.077 \pm 0.734\,\mathrm{PgC\,yr^{-2}}$ during the warming hiatus, with 54% of the simulated trends negative (Fig. 1h; P value < 0.01; Table 1). Therefore, we conclude that the apparent acceleration in net terrestrial C uptake over the warming hiatus is most likely due to diminished respiratory losses rather than increased photosynthetic gains.

What terrestrial C cycle processes are most sensitive to climate? To diagnose climate sensitivity, we investigated the correlation coefficient and the slope (γ) of the relationship between terrestrial C cycle processes and land temperature anomalies over the last three decades. Our results indicate that land temperature is significantly more correlated with TER than with GPP or NBP (Supplementary Table 1). While there are no statistically strong correlations between land temperature anomalies and NBP (Supplementary Table 1), we see that γ_{NBP} is consistently negative and varies between $-2.92\,\mathrm{PgC\,yr^{-1}}$ per °C during the warming period and $-5.31\,\mathrm{PgC\,yr^{-1}}$ per °C during the warming hiatus, suggesting that positive temperature anomalies at inter-annual to decadal timescales tend to suppress net terrestrial C uptake (Fig. 2a). In contrast, there are significant relationships between land temperature and GPP over the entire period of observation ($r = 0.51$; P value $= 0.0035$; DF $= 30$) and the warming period ($r = 0.55$; $P = 0.0226$; DF $= 16$), but not over the warming hiatus (Supplementary Table 1). However, the climate sensitivity of GPP has changed from positive $\gamma_{\mathrm{GPP}} = 6.48\,\mathrm{PgC\,yr^{-1}}$ per °C during the warming period to slightly negative $\gamma_{\mathrm{GPP}} = -1.26\,\mathrm{PgC\,yr^{-1}}$ per °C during the warming hiatus (Fig. 2b). A strong correlation is observed between TER and land temperature anomalies ($r = 0.57$; $P = 0.0007$; DF $= 30$) and this relationship is even stronger during the warming period ($r = 0.73$; $P = 0.0009$; DF $= 16$), but becomes insignificant during the warming hiatus ($r = 0.32$; $P = 0.24$; DF $= 14$) (Supplementary Table 1). While the correlation coefficients are not statistically distinguishable between these periods, the temperature sensitivity of total respiration (that is, γ_{TER}) is consistently positive from the warming period $9.40\,\mathrm{PgC\,yr^{-1}}$ per °C through the warming hiatus $4.05\,\mathrm{PgC\,yr^{-1}}$ per °C, indicating a strong and persistent positive terrestrial respiration response to warm temperature anomalies (Fig. 2c). These findings suggest that total ecosystem respiration is more sensitive to inter-annual to decadal scale temperature variability than primary productivity at the global scale and thus is likely to be the dominant process explaining much of the observed temperature sensitivity of the global C cycle[5].

How well do global land surface models perform at simulating terrestrial ecosystem respiration? Comparisons of total respiration estimated from observations with total respiration simulated by models of varying complexity reveal key differences that may help improve models (Fig. 3a). Our analysis revealed a significant decrease in cumulative change in TER between the warming period and the warming hiatus (Fig. 3b). The TRENDY ensemble of dynamic global vegetation models (DGVMs) that use historical climate data to calculate TER[16] also show a significant decrease in cumulative respiration change over the warming hiatus (Fig. 3b), albeit not as pronounced as our TER estimates. In contrast, the Coupled Model Intercomparison Project (CMIP5)[17] simulations, in which respiration is calculated from prognostic climate variables, actually show a slight increase in cumulative TER over the warming

Table 1 | Trend statistics for processes in the global C cycle and their change during the warming period and warming hiatus.

	Period of common observations (1982–2012)		Warming period (1982–1998)		Warming hiatus (1998–2012)	
	Trend (PgC yr^{-2})	*P* values	Trend (PgC yr^{-2})	s.d.	Trend (PgC yr^{-2})	s.d.
GPP	0.136†	0.006	0.328	±0.602	0.042	±0.730
NBP*	0.026†	0.010	**−0.007**	**±0.065**	**0.119**†	**±0.071**
TER	0.110†	0.005	**0.335**	**±0.605**	**−0.077**†	**±0.734**

Reported are Mann–Kendall trend statistics and their Sen's slopes with standard deviations for gross primary productivity (GPP), net biome productivity (NBP), and total ecosystem respiration (TER). Trend statistics are calculated from 4,500 simulations with error of GPP, NBP and TER; median values of trend statistics are reported for the period of common of observation (1982–2012), the warming period (1982–1998), and the warming hiatus (1998–2012). *Trend statistics for NBP are reported for the entire period of direct atmospheric observations (1959–2012). Processes with significant Sen's slopes are indicated by '†'. Significant differences in trends are indicated in bold where NBP shows a significant increase during the warming hiatus (two-tailed; *t*-statistic = 5.39; *P* value < 0.01; DF = 29), GPP shows no significant increase (one-tailed; *t*-statistic = 1.19; *P* value > 0.10; DF = 27), and TER shows a significant decrease (one-tailed; *t*-statistic = 1.80; *P* value < 0.05; DF = 27).

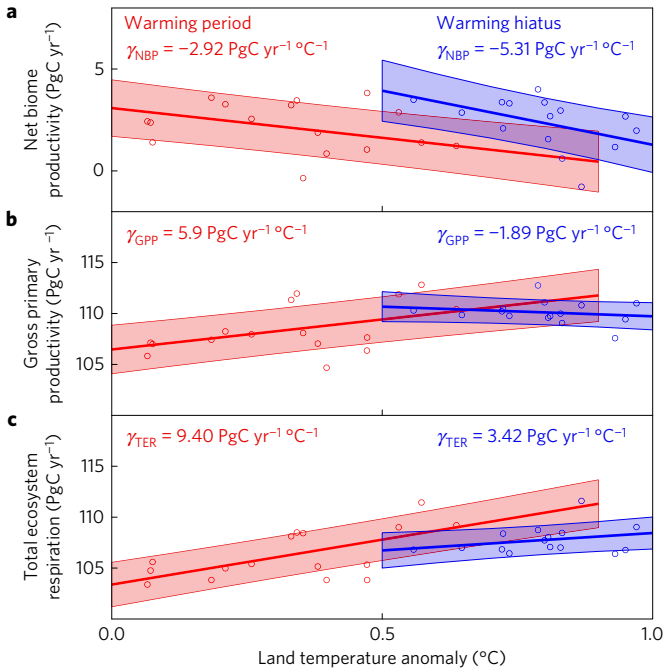

Figure 2 | Climate sensitivity of terrestrial carbon cycle processes over the last three decades. a, Plot showing net biome productivity (NBP), where γ_{NBP} represents the temperature sensitivity of NBP over the warming period (red) and the warming hiatus (blue). **b**, Plot showing gross primary productivity (GPP), where γ_{GPP} represents the temperature sensitivity of GPP over the warming period (red) and the warming hiatus (blue). **c**, Plot showing terrestrial ecosystem respiration (TER), where γ_{GPP} represents the temperature sensitivity of TER over the warming period (red) and the warming hiatus (blue). Open circles represent median values of 4,500 simulations of carbon cycle process and median annual values from 3 different land temperature records[42,43,45] over the warming period (red open circles) and the warming hiatus (blue open circles including 1998). Transparent confidence intervals (±1 σ) are plotted around carbon cycle temperature sensitivity slopes.

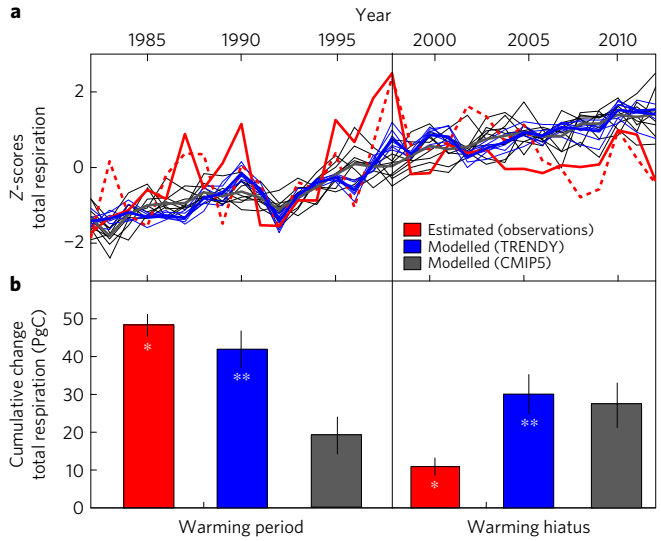

Figure 3 | Total respiration estimated from observations and simulated from models. a, *Z*-scores of total respiration calculated from observations (red solid line) and total respiration predicted empirically from global soil moisture and temperature data sets (red dashed line), compared with nine CMIP5 simulations (thin black lines), seven dynamic global vegetation TRENDY simulations (thin blue lines), and thick mean lines. **b**, Cumulative change in total respiration for the warming period (1984 through 1998) and the warming hiatus (1998 through 2012), where all estimates are normalized to comparable 15-year intervals and normalized to mean values at the start of each interval. A significant decrease in cumulative total respiration occurred for observed estimates (*red bars; *t*-statistic = 17.3; *P* value = 0.0065; DF = 26) and modelled estimates from the TRENDY ensemble (**blue bars, *t*-statistic = 2.9; *P* value = 0.0258; DF = 6), whereas no significant change in CMIP5 ensemble simulations occurred (*P* value = 0.6306; *t*-statistic = 0.5; DF = 8). Error bars represent bootstrapped standard deviations for model simulations and the standard error across estimates from observations, with simulated error (N = 4,500).

hiatus (Fig. 3b). The fact that suppressed respiration rates over the warming hiatus were simulated by DGVMs but not accurately simulated by ESMs suggests that the temperature sensitivity of respiration may be fairly well represented in land surface models but that the inability of ESMs to capture quasi-decadal temperature variability[15] may lead to biases in predictions of net terrestrial C mass balance on decadal timescales.

The DGVM simulations do show suppressed cumulative respiration over the warming hiatus; however, they do not show the slight decline evident in our TER estimates. This suggests that environmental factors important in regulating respiration may not be properly included in DGVM simulations. In fact, DGVM simulations of TER show strong correlations with temperature in most regions of the globe (Supplementary Fig. 8a), suggesting that DGVM simulations of TER are perhaps overly sensitive to temperature, especially in the tropics (Supplementary Fig. 8b), and not sensitive enough to other environmental variables known to control respiration[18]. While DGVMs show a fairly consistent TER response to changes in carbon supply through GPP and temperature, they tend to differ in their sensitivity of TER to soil moisture[19], which is a prognostic variable in DGVMs. To diagnose the sensitivity of TER to C supply, soil temperature and soil moisture, we adapted an empirical model of soil respiration to the global scale (see Methods). If we consider the well-established model of soil respiration (R_s)[8] as a function of soil C and soil temperature (Methods R_s^{temp} (equation (4))), we see a fairly strong

relationship between our independent TER estimate and the R_s^{temp} model ($r = 0.58$; $P = 0.0007$; normalized RMSE = 0.91). However, if we include soil moisture[20] into our global empirical model[21] (Methods $R_s^{temp+moist}$ (equation (5))), we see an improved relationship ($r = 0.61$; $P = 0.0003$; normalized RMSE = 0.87) (Supplementary Fig. 6) that more closely parallels our TER estimates over the warming hiatus (Fig. 3a; dashed red line). This slight decline in soil respiration derived from our empirical $R_s^{temp+moist}$ model is the result of relatively flat temperatures over the warming hiatus[15] in combination with the continued decline in observed soil moisture globally[22] that is not predicted by DGVM models (Supplementary Fig. 7). Thus, DGVM simulations of respiration may be accurately capturing temperature sensitivity as forced directly by climate data, but their inconsistent response to internally predicted soil moisture may explain the slight divergence between model simulations and observationally constrained estimates of respiration. However, recent evidence of acclimation of autotrophic respiration would suggest that the relationship between temperature and respiration may vary over time and that a constant Q_{10} relationship may not be appropriate to describe autotrophic respiration[23]. It is also worth noting that we are using recently developed gridded soil C and satellite-derived soil moisture data products (Methods) with limited spatial and depth extent that may restrict their incorporation into land surface models. Nonetheless, our analysis suggests that land surface models, when forced with observed temperature data, capture some of the reduced respiration observed over the warming hiatus, but that soil moisture may help reconcile respiration estimates from models and estimates constrained by global observations.

Our analysis identifies total ecosystem respiration as the likely process regulating the relationship between variability in land temperature and atmospheric CO_2[3,5]. In our attempt to disentangle major photosynthetic and respiration pathways in the global C cycle, however, we have greatly oversimplified important processes that contribute to TER. At the ecosystem scale, total respiration is comprised of autotrophic respiration that integrates growth and maintenance respiration, which are sensitive to C supplied through primary productivity rates and temperature changes[24], as well as heterotrophic respiration, which is sensitive to temperature and moisture[25]. A comparison of our top-down TER estimates with a global database of soil respiration studies[8] revealed that our overall trend in TER 0.11 PgC yr^{-2} is statistically indistinguishable from the reported trend in global soil respiration of 0.1 PgC yr^{-2} that has been attributed to surface warming[8] (Supplementary Fig. 5). The absolute values of our top-down TER estimates (106 ± 12 PgC yr^{-1}; mean $\pm$ σ) are only slightly higher than the bottom-up globally extrapolated soil respiration estimates (98 ± 12 Pg C yr^{-1}), suggesting that about 90% of TER is coming from soil respiration. However, estimates of GPP from observations and models vary widely from 112 to 169 PgC yr^{-1} (ref. 26), so if we use the independent estimate of GPP $= 123 \pm 8$ extrapolated from a global array of flux towers[27], we estimate that approximately 80% of TER is from soil respiration, which is more in the range of ecosystem-scale studies, assuming that most of the autotrophic respiration is from roots below ground[28]. This suggests that our global GPP estimates derived from satellite observations are on the low range, resulting in a possibly global TER estimate that is biased low. However, how much autotrophic respiration comes from below ground versus above ground probably varies considerably among ecosystems and remains an open question at the global scale. Nevertheless, independent GPP estimates show a similar levelling off over the warming hiatus (Supplementary Fig. 3), suggesting that the observed acceleration in the rate of net terrestrial C uptake during the warming hiatus is robust and not due to increased C gains from photosynthesis, but rather reduced respiration.

Soil moisture appears to be a strong second-order control on respiration and in the absence of temperature variability soil moisture may emerge as the dominant environmental control on respiration (Fig. 3a). Indeed, ecosystem-scale studies have identified optimum soil moisture values for maximum soil respiration[20], and a global assessment of soil respiration studies identified mean annual precipitation as the second best predictor of soil respiration after temperature[8]. Thus, it is possible that soil moisture is an important direct factor regulating heterotrophic respiration and precipitation is an important indirect factor in regulating autotrophic respiration by supplying C through photosynthesis[29] and that soil respiration integrates both of these respiration pathways.

Our estimate of TER implicitly includes other major C loss pathways from the biosphere, such as fire emissions (2 to 3 PgC yr^{-1})[30] and evasion of CO_2 from inland waters (2.1 PgC yr^{-1})[31]; however, these C loss pathways are two orders of magnitude less than our TER estimates and show no obvious trends according to available global estimates. Therefore, these C loss pathways are probably not contributing greatly to decadal variability in our TER estimates. While our analysis helps identify major global C cycle pathways that may be sensitive to climate, more detailed ecosystem-scale studies and models are required to identify the specific metabolic mechanisms contributing to the sensitivity of respiration to temperature and moisture.

Using satellite and atmospheric data in a complementary way to estimate total respiration provides new insight to help reconcile previous global C cycle studies. First of all, the only way to resolve an apparent deceleration in primary productivity[32] and an acceleration in net biome productivity in recent decades[33] is for TER to remain constant or decrease. Indeed, according to observations and DGVM simulations, TER has remained fairly constant over the warming hiatus. Second, it has been hypothesized that the observed increase in NBP following the eruption of Mount Pinatubo in 1991 was the result of increased photosynthesis in response to more diffuse light[34], and/or diminished respiration in response to cooler temperatures[35]. Our results indicate that TER was reduced several years following the eruption. These observations are supported by both ESM and DGVM simulations forced with volcanic cooling effects but not diffuse light effects that show a clear reduction in total respiration following the eruption of Mount Pinatubo (Fig. 3). This is also consistent with previous model results showing increased boreal forest NBP following the Mount Pinatubo eruption as a result of decreased heterotrophic respiration[35]. In contrast, the major El Niño events of 1987 and 1998 are associated with positive land temperature anomalies and reduced NBP globally. During these events global GPP shows very little change (Fig. 1), whereas TER appears to have increased in response to both El Niño events. These results are not necessarily consistent with recent DGVM simulations suggesting that much of the inter-annual variability in the terrestrial C cycle is governed by primary productivity in semi-arid ecosystems[36]. While our GPP estimates show very little inter-annual variability, they are largely driven by the observed fraction of photosynthetically active radiation and a light use efficiency model that is sensitive to temperature and atmospheric water vapour. Although this satellite-informed model has been validated across an array of eddy-flux sites, it may not accurately represent the response of semi-arid ecosystems to inter-annual climate variability. Therefore, additional ecosystem studies exploring the response of primary productivity and total respiration to changing environmental variables, especially in semi-arid ecosystems, is necessary to better align models and observations of the global C cycle.

In conclusion, net terrestrial C uptake clearly accelerated during the warming hiatus most likely due to reduced respiration and not increased photosynthesis, thus preventing a large fraction of terrestrial C from returning to the atmosphere. As warming

trends resume[37], however, we would expect a greater fraction of terrestrial C to return to the atmosphere. Although recent evidence indicates acclimation of both plant photosynthesis and respiration at higher temperatures[23,38], the net effect of this acclimation response has the potential to sustain future terrestrial C uptake[39,40]. Therefore, this vital ecosystem service provided by the terrestrial biosphere of removing a large fraction of CO_2 emissions from the atmosphere has been mediated by decadal variability in the balance of photosynthesis and respiration in response to decadal temperature variability.

Methods

Methods, including statements of data availability and any associated accession codes and references, are available in the online version of this paper.

Received 10 May 2016; accepted 15 December 2016; published online 23 January 2017

References

1. Le Quéré, C. *et al*. Global carbon budget 2014. *Earth Syst. Sci. Data* **7,** 47–85 (2015).
2. Friedlingstein, P. *et al*. Uncertainties in CMIP5 climate projections due to carbon cycle feedbacks. *J. Clim.* **27,** 511–526 (2014).
3. Bacastow, R. *et al*. Atmospheric carbon dioxide, the Southern Oscillation, and the weak 1975 El Niño. *Science* **210,** 66–68 (1980).
4. Bousquet, P. *et al*. Regional changes in carbon dioxide fluxes of land and oceans since 1980. *Science* **290,** 1342–1346 (2000).
5. Cox, P. M. *et al*. Sensitivity of tropical carbon to climate change constrained by carbon dioxide variability. *Nature* **494,** 341–344 (2013).
6. Anderegg, W. R. L. *et al*. Tropical nighttime warming as a dominant driver of variability in the terrestrial carbon sink. *Proc. Natl Acad. Sci. USA* **112,** 15591–15596 (2015).
7. Doughty, C. E. & Goulden, M. L. Are tropical forests near a high temperature threshold? *J. Geophys. Res.* **113,** G00B07 (2008).
8. Bond-Lamberty, B. & Thomson, A. Temperature-associated increases in the global soil respiration record. *Nature* **464,** 579–582 (2010).
9. Hoffman, F. M. *et al*. Causes and implications of persistent atmospheric carbon dioxide biases in Earth System Models. *J. Geophys. Res.* **119,** 141–162 (2014).
10. Smith, W. K. *et al*. Large divergence of satellite and Earth system model estimates of global terrestrial CO_2 fertilization. *Nat. Clim. Change* **6,** 306–310 (2016).
11. Schulze, E.-D., Wirth, C. & Heimann, M. Managing forests after Kyoto. *Science* **289,** 2058–2059 (2000).
12. Chapin, F. III *et al*. Reconciling carbon-cycle concepts, terminology, and methods. *Ecosystems* **9,** 1041–1050 (2006).
13. Ballantyne, A. *et al*. Audit of the global carbon budget: estimate errors and their impact on uptake uncertainty. *Biogeosciences* **12,** 2565–2584 (2015).
14. Fyfe, J. C., Gillett, N. P. & Zwiers, F. W. Overestimated global warming over the past 20 years. *Nat. Clim. Change* **3,** 767–769 (2013).
15. Marotzke, J. & Forster, P. M. Forcing, feedback and internal variability in global temperature trends. *Nature* **517,** 565–570 (2015).
16. Sitch, S. *et al*. Recent trends and drivers of regional sources and sinks of carbon dioxide. *Biogeosciences* **12,** 653–679 (2015).
17. Taylor, K. E., Stouffer, R. J. & Meehl, G. A. An overview of CMIP5 and the experiment design. *Bull. Am. Meteorol. Soc.* **93,** 485–498 (2012).
18. Davidson, E. A. & Janssens, I. A. Temperature sensitivity of soil carbon decomposition and feedbacks to climate change. *Nature* **440,** 165–173 (2006).
19. Sulman, B. N. *et al*. Impact of hydrological variations on modeling of peatland CO_2 fluxes: results from the North American Carbon Program site synthesis. *J. Geophys. Res.* **117,** G01031 (2012).
20. Davidson, E. A., Samanta, S., Caramori, S. S. & Savage, K. The dual Arrhenius and Michaelis–Menten kinetics model for decomposition of soil organic matter at hourly to seasonal time scales. *Glob. Change Biol.* **18,** 371–384 (2012).
21. Chen, S., Zou, J., Hu, Z., Chen, H. & Lu, Y. Global annual soil respiration in relation to climate, soil properties and vegetation characteristics: summary of available data. *Agric. For. Meteorol.* **198,** 335–346 (2014).
22. Jung, M. *et al*. Recent decline in the global land evapotranspiration trend due to limited moisture supply. *Nature* **467,** 951–954 (2010).
23. Reich, P. B. *et al*. Boreal and temperate trees show strong acclimation of respiration to warming. *Nature* **531,** 633–636 (2016).
24. Piao, S. *et al*. Forest annual carbon cost: a global-scale analysis of autotrophic respiration. *Ecology* **91,** 652–661 (2010).
25. Suseela, V., Conant, R. T., Wallenstein, M. D. & Dukes, J. S. Effects of soil moisture on the temperature sensitivity of heterotrophic respiration vary seasonally in an old-field climate change experiment. *Glob. Change Biol.* **18,** 336–348 (2012).
26. Anav, A. *et al*. Spatiotemporal patterns of terrestrial gross primary production: a review. *Rev. Geophys.* **53,** 785–818 (2015).
27. Beer, C. *et al*. Terrestrial gross carbon dioxide uptake: global distribution and covariation with climate. *Science* **329,** 834–838 (2010).
28. Luyssaert, S. *et al*. CO_2 balance of boreal, temperate, and tropical forests derived from a global database. *Glob. Change Biol.* **13,** 2509–2537 (2007).
29. Högberg, P. *et al*. Large-scale forest girdling shows that current photosynthesis drives soil respiration. *Nature* **411,** 789–792 (2001).
30. van der Werf, G. R. *et al*. Interannual variability in global biomass burning emissions from 1997 to 2004. *Atmos. Chem. Phys.* **6,** 3423–3441 (2006).
31. Raymond, P. A. *et al*. Global carbon dioxide emissions from inland waters. *Nature* **503,** 355–359 (2013).
32. Zhao, M. & Running, S. W. Drought-induced reduction in global terrestrial net primary production from 2000 through 2009. *Science* **329,** 940–943 (2010).
33. Sarmiento, J. L. *et al*. Trends and regional distributions of land and ocean carbon sinks. *Biogeosciences* **7,** 2351–2367 (2010).
34. Gu, L. *et al*. Response of a deciduous forest to the Mount Pinatubo eruption: enhanced photosynthesis. *Science* **299,** 2035–2038 (2003).
35. Lucht, W. *et al*. Climatic control of the high-latitude vegetation greening trend and Pinatubo effect. *Science* **296,** 1687–1689 (2002).
36. Ahlström, A. *et al*. The dominant role of semi-arid ecosystems in the trend and variability of the land CO_2 sink. *Science* **348,** 895–899 (2015).
37. England, M. H., Kajtar, J. B. & Maher, N. Robust warming projections despite the recent hiatus. *Nat. Clim. Change* **5,** 394–396 (2015).
38. Smith, N. G., Malyshev, S. L., Shevliakova, E., Kattge, J. & Dukes, J. S. Foliar temperature acclimation reduces simulated carbon sensitivity to climate. *Nat. Clim. Change* **6,** 407–411 (2016).
39. Lombardozzi, D. L., Bonan, G. B., Smith, N. G., Dukes, J. S. & Fisher, R. A. Temperature acclimation of photosynthesis and respiration: a key uncertainty in the carbon cycle-climate feedback. *Geophys. Res. Lett.* **42,** 8624–8631 (2015).
40. Huntingford, C. *et al*. Simulated resilience of tropical rainforests to CO_2-induced climate change. *Nat. Geosci.* **6,** 268–273 (2013).
41. Harris, I., Jones, P., Osborn, T. & Lister, D. Updated high-resolution grids of monthly climatic observations–the CRU TS3. 10 Dataset. *Intl J. Climatol.* **34,** 623–642 (2014).
42. *Team G. GISS Surface Temperature Analysis* (*GISTEMP*) (NASA Goddard Institute for Space Studies, accessed 13 May 2015); http://data.giss.nasa.gov/gistemp
43. Vose, R. S. *et al*. NOAA's merged land–ocean surface temperature analysis. *Bull. Am. Meteorol. Soc.* **93,** 1677–1685 (2012).
44. Running, S. W. *et al*. A continuous satellite-derived measure of global terrestrial primary production. *Bioscience* **54,** 547–560 (2004).
45. Jones, P. *et al*. Hemispheric and large-scale land-surface air temperature variations: an extensive revision and an update to 2010. *J. Geophys. Res.* **117,** D05127 (2012).

Acknowledgements

This work was stimulated by a workshop on abrupt changes in the global carbon cycle sponsored by Princeton University and the The Finnish Society of Sciences and Letters. Further support for this research was provided by NSF-DEB no. 1550932 and USDA no. MONZ-1302. W.R.L.A. was supported by a NOAA global change fellowship and W.K.S. was supported by a Luc Hoffman Fellowship. Satellite observations and MOD-17 algorithm development were supported by NASA grant NNX08AG87A to S.W.R. We are also grateful to the global citizens and NOAA scientists who have helped maintain the global atmospheric CO_2 observation network. This work was greatly improved through input from colleagues D. Lombardozzi and B. Sullivan.

Author contributions

This study was conceived of at a workshop hosted by J.S. and P.K. and the study was designed by A.B., W.A. and W.S. Atmospheric data were analysed by A.B. and P.T. The compilation and analysis of satellite data was conducted by W.S. and S.R. Simulation data from ESMs were accessed and analysed by A.A., P.F. and E.S. and simulation data from DGVMs was provided by B.P. All authors contributed during the writing of the paper.

Additional information

Supplementary information is available in the online version of the paper. Reprints and permissions information is available online at www.nature.com/reprints. Correspondence and requests for materials should be addressed to A.B.

Competing financial interests

The authors declare no competing financial interests.

Methods

Gross primary productivity (GPP) estimates. GPP is estimated from satellite observations combined with meteorological data[44], such that:

$$\mathrm{GPP} = \mathrm{FPAR} \times \mathrm{PAR} \times \mathrm{LUE}_{\max} \times f(T_{\min}) \times f(\mathrm{VPD}) \quad (2)$$

where the fraction of photosynthetically active radiation absorbed (FPAR) is estimated from continuous measurements of normalized difference vegetation index (NDVI) obtained from the Moderate Resolution Imaging Spectrometer (MODIS; 2000 to 2012) and its predecessor the Advanced Very High Resolution Radiometer (AVHRR; 1982 to 2006)[46], and multiplied by photosynthetically active radiation (PAR). The amount of actual absorbed photosynthetically active radiation (that is, FPAR × PAR) is then multiplied by maximum light use efficiencies ($\mathrm{LUE}_{\max}$), minimum temperature functions (f ($T_{\min}$)), and vapour pressure deficit functions (f (VPD)), which vary according to 13 different land cover types[47] to yield annual GPP estimates using the MOD-17 algorithm[47]. While the LUE model used here to translate satellite FPAR observations into a currency of carbon flux has been criticized for being overly sensitive to temperature[48], it has been validated with reasonable success across a global array of eddy-flux tower sites[49]. This LUE model approach does not necessarily agree with plot-based estimates of productivity in tropical locations[50], but tends to provide better estimates in ecosystems with greater seasonal variability at high latitudes[49]. Comparison of our LUE-based estimates of GPP with independent GPP global estimates up-scaled from eddy-flux calculations[51] revealed differences in the absolute values of annual GPP but not appreciable differences in decadal trends that are the focus of this analysis (Supplementary Fig. 3). While this favourable comparison is not surprising given that the MOD-17 algorithm has been calibrated and validated against eddy-flux sites and the up-scaled eddy-flux estimates use satellite and meteorological data to extrapolate globally, it does corroborate our trends in GPP and suggest that they are the result of changes in absorbed photosynthetically active radiation and not an artefact of meteorological variables included in the model. The two main sources of error in estimating GPP globally using the MOD-17 are algorithm error and instrument error. Most of the algorithm error arises from the globally gridded meteorological data sets of PAR, VPD and $T_{\min}$ required to estimate climate-driven reductions in vegetation light use efficiency. To test the sensitivity of GPP calculations to meteorological data sets, we calculated global annual GPP estimates from three of the most commonly used meteorological data sets: National Centers for Environmental Prediction/National Center for Atmospheric Research (NCEP/NCAR) reanalysis; NASA Data Assimilation Office (DAO); and European Center for Medium-Range Weather Forecasting (ECMWF) according to Zhao and colleagues[52]. The standard deviation of these annual GPP estimates was then re-sampled 1,000 times to generate an error distribution with a mean of 22.0 PgC yr^{-1} (2σ). It is important to note that the absolute magnitude of annual GPP estimates may vary considerably depending on the meteorological data set used but annual GPP anomalies tend to be consistent across meteorological data sets at the global scale, such that anomalously high annual GPP estimates tend to be high regardless of the meteorological data set used. Thus, the temporal variability in annual global GPP estimates is driven primarily by changes in observed FPAR[10,52]. To estimate instrument error the standard deviation of global annual GPP estimates obtained independently from MODIS and AVHRR satellites using NCEP/NCAR reanalysis data during the overlap period of observation (2000–2006) was re-sampled 1,000 times to calculate a mean instrument error corresponding to 1.7 PgC yr^{-1} (2σ). There was no difference in trends for the two satellite observations of global annual FPAR indicating no evidence of satellite bias in the record. Instrument degradation is likely over time and may lead to temporally increasing uncertainties in FPAR; however, instrument error is an order of magnitude less than algorithm error. Total error values were then randomly drawn from our joint distribution of algorithm and instrument errors and added to mean annual GPP calculated from MODIS using the latest Global Inventory Modeling and Mapping Studies (GIMMS) 3G data set[46]. A matrix of 4,500 simulated GPP time series with error were then differenced from our array of 4,500 NBP estimates to calculate 4,500 simulations of TER with error.

Net biome productivity (NBP) estimates. Global terrestrial NBP is inferred as the residual land sink[53] with errors propagated according to Ballantyne *et al.*[13], such that:

$$\mathrm{NBP} = \Sigma E - \mathrm{d}C/\mathrm{d}t - N_{\mathrm{O}} \quad (3)$$

where according to mass balance, NBP must be equivalent to the sum of fossil-fuel and land-use emissions to the atmosphere (ΣE) minus the atmospheric CO_2 growth rate ($\mathrm{d}C/\mathrm{d}t$) and net ocean C uptake (N_{O}). While several C loss pathways from the biosphere to the atmosphere exist and several of these pathways, such as fire emissions and CO_2 evasion from inland waters[31,54], rival the magnitude of NBP, if this C is lost from the biosphere and does not remain in the atmosphere we must conclude that it was taken up by the land or ocean. For the atmospheric growth rate, errors are calculated due to the spatial heterogeneity and sampling bias in the global atmospheric observing network (NOAA/ESRL). This is done by re-sampling the observation network within the marine boundary layer 100 times, with at least one site selected from the Northern Hemisphere, Southern Hemisphere and Tropics, to construct artificial observation networks of 40 sites[55]. From these artificial networks the atmospheric growth rate is calculated as the difference between mean December and January values of the current year and the mean December and January values of the previous year among all sites and then the median value across sampling networks is reported with a 2σ uncertainty. Standard deviations between the atmospheric growth rate calculated across the global atmospheric observing network (1980–2012) and the growth rate calculated from just Mauna Loa and the South Pole (1959–2012) were calculated over the period of common observation and added as uncertainty to the period prior to 1980. Estimates of fossil-fuel emissions, including cement production, to the atmosphere were obtained from three separate emission inventories—the Carbon Dioxide Information and Analysis Center (CDIAC), the Emissions Database for Global Atmospheric Research (EDGAR), and BP statistics (BP). Although these inventories rely on similar energy consumption statistics, their protocols for the treatment of bunker fuels and gas flaring, as well as emission factors of CO_2 by fuel type, vary considerably resulting in different global emission estimates. To estimate emission errors, national emission estimates were tabulated and errors were drawn from a random distribution of errors[56] from countries grouped by UN development classes[13]. Our novel 'el camino' approach is different in that emission errors are temporally correlated from year to year thus following a path, in contrast to the conventional Monte-Carlo approach that assumes errors are independent from year to year. These random errors were then used to scale the temporally autocorrelated noise with 20-year persistence, which was then added to the emission estimates of each country. Country-level emission estimates were then aggregated into arrays of 500 simulations of global emissions for each of the three inventories for a grand total of 1,500 simulated time series of fossil-fuel emission estimates ($3 \times 500 = 1{,}500$), spanning the period from 1959 to 2012. Land-use emissions were estimated using a similar approach from three different inventories[57–59], where temporally autocorrelated random noise with a 5-year persistence corresponding to the update interval of deforestation/regrowth statistics[60] was scaled to a reported 2σ error of ± 0.5 PgC yr^{-1}, and arrays of 500 time series were simulated for each of the three land-use inventories ($3 \times 500 = 1{,}500$). Land-use legacies, especially in countries that have already undergone industrialization, can lead to biases in estimates of net terrestrial C uptake[61]. However, it is worth noting here that the apparent acceleration in NBP since 1998 is probably not due to land-use legacies because at the global scale land-use emissions show no significant trend over the last five decades[62] and appear to have decreased slightly since 1998, albeit with some uncertainties[63]. Therefore, the apparent increase in NBP since 1998 is the result of increasing fossil-fuel emissions that are not remaining in the atmosphere[64] and not the result of appreciable changes in land-use emissions. Land-use emission arrays were combined with each of our fossil-fuel emission arrays for a total emission matrix of 4,500 simulations ($3 \times 3 \times 500 = 4{,}500$). Net ocean C uptake was estimated by simulating 900 realizations of N_{O} from 5 different ocean biogeochemical model simulations[53] where random 2σ error of 1.2 PgC yr^{-1} was added to each model simulation based on decadal measurements of atmospheric O_2[65,66] for a matrix of 4,500 simulations of N_{O} ($5 \times 900 = 4{,}500$)[65,66]. Our net ocean uptake matrix was then subtracted from our total emissions matrix and then atmospheric growth rates were randomly drawn from our simulated global observing network and subtracted to yield 4,500 estimates of NBP simulated with error from 1959 to 2012 (ref. 13).

Model simulations of global total respiration (TER). Our empirically derived estimates of TER were compared with simulated values of TER from an ensemble of ESM simulations from the Coupled Model Intercomparison Project Phase 5 (CMIP5) and an ensemble of DGVM simulations included in the TRENDY archive[16]. While many of these DGVMs are embedded as the land model component of these ESMs, the DGVM simulations are forced by atmospheric and climate variables, whereas the ESM simulations have climate and atmospheric variables (except volcanic aerosols) as prognostic variables. By looking at these quasi-independent simulations we can isolate the extent to which climate versus ecosystem response explain mismatches between TER calculated from observations and TER simulated from models.

From ESM simulations TER was calculated as the difference between GPP and NBP from the CMIP5 archive, which combined historic hindcasts with future projections of climate and carbon dynamics into continuous experiments spanning 1900–2100. A total of nine ESM model simulations—BCC-CSM-1, BNU-ESM, CanESM2, CESM1-BGC, IPSL-CM5A-MR, IPSL-CM5A-LR, MIROC-ESM, MIROC-ESM-CHEM and NorESM-M, were considered in our analysis. From this, we extracted years 1982 to 2012 for comparison with our inferred estimates of TER. As these models vary between 20 and 40% in their mean estimates of TER, individual model estimates were normalized and reported as z-scores to compare relative changes in TER trends among models and observations.

Estimates of TER were also derived from DGVM-simulated responses of autotrophic and heterotrophic respiration (excluding fire), to climate and CO_2. Autotrophic respiration was not a mandatory output for the models, and so was

calculated as the difference between net primary production and gross primary production. An ensemble of seven state-of-the-art DGVMs were analysed: LPJ[67], LPJ-GUESS[68], JULES-TRIFFID[69], SDGVM[70], OCN[71], ORCHIDEE[72] and NCAR-CLM4CN[73]. The model ensemble stem from the TRENDY Inter-model Comparison ('Trends in net land–atmosphere carbon exchange over the period 1980–2010') that provided bottom-up estimates of carbon cycle processes for the Regional Carbon Cycle Assessment and Processes (RECCAP)[16]. Our analysis uses simulations from the 'S2' storyline that includes time-varying atmospheric CO_2 concentrations and climate and fixed land cover for 2005. All simulations were based on climate forcing from the CRU-NCEPv4 climate variables at 6-h resolution for the years 1901–2012, including precipitation, snowfall, temperature, short-wave and long-wave radiation, specific humidity, air pressure and wind speed. Global atmospheric CO_2 was provided as an annual time series reconstructed from ice-core measurements and then merged with atmospheric observations starting in 1956 from the Mauna Loa record. Land use distinguished between managed crops and natural vegetation using a common database with land use fixed for the year 2005 for all simulations included in our analysis. Soil databases specific to each team were used to specify soil texture, water holding capacity, and thermal diffusivity properties. Modelling groups also individually determined the treatment of vegetation dynamics and disturbance, using either static or dynamic plant functional types and including or excluding disturbance (mainly fire). Models were spun-up to equilibrate soil and vegetation carbon pools for pre-industrial conditions (typically 1,000–3,000 years) by recycling climate mean and variability for years 1901–1920.

Lastly, to reconcile TER estimates constrained from global observations with TER simulations from DGVMs we conducted a simple sensitivity experiment comparing empirical respiration models. Assuming that a large fraction of TER is composed of soil respiration (R_s), we predicted global soil respiration in response to soil C content (C_s) and soil temperature (T_s), according to models previously validated against a global database of R_s observations[74]:

$$R_s^{\text{temp}} = C_s \times 64 \times (1.72^{0.21 \times T_s}) \quad (4)$$

as well as R_s as a function of C_s, T_s, and soil moisture (M_s):

$$R_s^{\text{temp+moist}} = C_s \times 64 \times (1.72^{0.21 \times T_s}) \times \left(\frac{M_s + 2.1}{0.55 - 2.1}\right)^{6.6481} \times \left(\frac{M_s + 0.007}{0.55 - 0.007}\right)^{3.22} \quad (5)$$

These independent empirical estimates of R_s were then compared with our observationally constrained estimates of TER. As inputs to our model we used a globally harmonized soil C database[75], the European Space Agency's remotely sensed merged soil moisture data product (http://www.esa-soilmoisture-cci.org/node/145), and land surface temperatures[41]. Due to the slight differences in magnitude of TER and R_s we compared estimates using root mean squared error (RMSE) on normalized z-scores and thus the reported RMSE values are unitless and annual values were aggregated for global estimates of R_s.

Statistical analyses. For our statistical analyses, Mann–Kendall non-parametric trend analyses were conducted to determine the statistical significance of any observed trends and then Sen's slope statistics were calculated with confidence intervals[76]. Trend statistics and slopes were calculated on each of our 4,500 simulated estimates of GPP, NBP and TER for the period of common observations (1982–2012), the warming period (1982–1998), and for the warming hiatus (1998–2012), and median values are reported (Table 1). As we were analysing differences in the distributions of trends from a large number of Monte Carlo simulations ($N = 4{,}500$) we could not use conventional Student's t-tests due to the overly inflated degrees of freedom ($N - 2 = 4{,}498$ for a one-tailed t-test). Instead we modified the Welch's t-test for unequal variances by using mean and variance values from the trends of our simulations (Fig. 1), but we calculated effective degrees of freedom from the years of observations ($N = 31$). By reducing the effective degrees of freedom we greatly raised the exceedance for a significant t-statistic value and reduced the odds of a type 1 statistical error.

Estimates of GPP, NBP and TER were compared with both observational and gridded temperature data. For temporal correlations between global C cycle processes and temperature we used mean land temperature anomaly data from CRUTEM[77], NASA-GISS[42] and NOAA[43]. There is considerable decadal variability in all land surface temperature records. While we recognize that the currently observed temperature hiatus is debated[78], it is clear that Earth's surface has not warmed continuously in response to anthropogenic perturbations to the atmosphere, but rather has followed a decadal stair-step pattern with several previous warming periods and warming hiatuses observed[79]. Here we use the so-called 'warming hiatus' as a global experiment to test the sensitivity of global C cycle processes to changes in surface warming. Our delineations of the warming period (1982–1998) and the warming hiatus (1998–2012) are arbitrary, but they correspond to two intervals of different land surface climate over which we have concurrent global measurements of atmospheric CO_2 and global satellite estimates of primary productivity.

Data availability. All data analysed in this study are publicly available. Satellite observations used for calculating GPP can be obtained from the Numerical Terradynamic Simulation Group data portal (http://www.ntsg.umt.edu/data). All data for estimating NBP are available through the Global Carbon Project[53], with errors estimated from a novel Bayesian fusion approach[80]. Simulated terrestrial carbon cycle data were obtained for ESMs from the CMIP5 archive accessed through the Earth System Grid Federation data portal (http://esgf.llnl.gov) and from DGVMs from the TRENDY archive[16]. Land surface temperature data used for calculating temperature sensitivity were obtained from three publicly available sources—Climate Research Unit (https://crudata.uea.ac.uk/cru/data/temperature), NASA Goddard Institute for Space Studies (http://data.giss.nasa.gov/gistemp) and NOAA (https://www.ncdc.noaa.gov/data-access/marineocean-data/noaa-global-surface-temperature-noaaglobaltemp).

References

46. Zhu, Z. *et al*. Global data sets of vegetation leaf area index (LAI) 3g and Fraction of Photosynthetically Active Radiation (FPAR) 3g derived from Global Inventory Modeling and Mapping Studies (GIMMS) Normalized Difference Vegetation Index (NDVI3g) for the period 1981 to 2011. *Remote Sensing* **5,** 927–948 (2013).
47. Zhao, M., Running, S., Heinsch, F. A. & Nemani, R. in *Land Remote Sensing and Global Environmental Change* (eds Ramachandran, B., Justice, C. O. & Abrams, M. J.) 635–660 (Springer, 2011).
48. Samanta, A. *et al*. Comment on 'Drought-induced reduction in global terrestrial net primary production from 2000 through 2009'. *Science* **333,** 1093 (2011).
49. Heinsch, F. A. *et al*. Evaluation of remote sensing based terrestrial productivity from MODIS using regional tower eddy flux network observations. *IEEE Trans. Geosci. Remote Sensing* **44,** 1908–1925 (2006).
50. Cleveland, C. C. *et al*. A comparison of plot-based satellite and Earth system model estimates of tropical forest net primary production. *Glob. Biogeochem. Cycles* **29,** 626–644 (2015).
51. Jung, M. *et al*. Global patterns of land-atmosphere fluxes of carbon dioxide, latent heat, and sensible heat derived from eddy covariance, satellite, and meteorological observations. *J. Geophys. Res.* **116** (2011).
52. Zhao, M., Running, S. W. & Nemani, R. R. Sensitivity of Moderate Resolution Imaging Spectroradiometer (MODIS) terrestrial primary production to the accuracy of meteorological reanalyses. *J. Geophys. Res.* **111,** G01002 (2006).
53. Le Quéré, C. *et al*. The global carbon budget 1959–2011. *Earth Syst. Sci. Data* **5,** 165–185 (2013).
54. van der Werf, G. R. *et al*. Global fire emissions and the contribution of deforestation, savanna, forest, agricultural, and peat fires (1997–2009). *Atmos. Chem. Phys.* **10,** 11707–11735 (2010).
55. Masarie, K. A. & Tans, P. P. Extension and integration of atmospheric carbon dioxide data into a globally consistent measurement record. *J. Geophys. Res.* **100,** 11593–11610 (1995).
56. Andres, R. J., Boden, T. A. & Higdon, D. A new evaluation of the uncertainty associated with CDIAC estimates of fossil fuel carbon dioxide emission. *Tellus B* **66,** 23616 (2014).
57. Houghton, R. A. Land-use change and the carbon cycle. *Glob. Change Biol.* **1,** 275–287 (1995).
58. Stocker, B., Strassmann, K. & Joos, F. Sensitivity of Holocene atmospheric CO_2 and the modern carbon budget to early human land use: analyses with a process-based model. *Biogeosciences* **8,** 69–88 (2011).
59. Jain, A. K., Meiyappan, P., Song, Y. & House, J. I. CO_2 emissions from land-use change affected more by nitrogen cycle, than by the choice of land-cover data. *Glob. Change Biol.* **19,** 2893–2906 (2013).
60. Friedlingstein, P. *et al*. Update on CO_2 emissions. *Nat. Geosci.* **3,** 811–812 (2010).
61. Erb, K.-H. *et al*. Bias in the attribution of forest carbon sinks. *Nat. Clim. Change* **3,** 854–856 (2013).
62. Ballantyne, A., Alden, C., Miller, J., Tans, P. & White, J. Increase in observed net carbon dioxide uptake by land and oceans during the past 50 years. *Nature* **488,** 70–72 (2012).
63. Morton, D. C. Forest carbon fluxes: a satellite perspective. *Nat. Clim. Change* **6,** 346–348 (2016).
64. Francey, R. J. *et al*. Atmospheric verification of anthropogenic CO_2 emission trends. *Nat. Clim. Change* **3,** 520–524 (2013).
65. Ishidoya, S. *et al*. Time and space variations of the O_2/N_2 ratio in the troposphere over Japan and estimation of the global CO_2 budget for the period 2000–2010. *Tellus B* **64,** 18964 (2012).
66. Manning, A. C. & Keeling, R. F. Global oceanic and land biotic carbon sinks from the Scripps atmospheric oxygen flask sampling network. *Tellus B* **58,** 95–116 (2006).
67. Sitch, S. *et al*. Evaluation of ecosystem dynamics, plant geography and terrestrial carbon cycling in the LPJ dynamic global vegetation model. *Glob. Change Biol.* **9,** 161–185 (2003).

68. Smith, B., Prentice, I. C. & Sykes, M. T. Representation of vegetation dynamics in the modelling of terrestrial ecosystems: comparing two contrasting approaches within European climate space. *Glob. Ecol. Biogeogr.* **10,** 621–637 (2001).
69. Cox, P. M., Huntingford, C. & Harding, R. J. A canopy conductance and photosynthesis model for use in a GCM land surface scheme. *J. Hydrol.* **212,** 79–94 (1998).
70. Woodward, F. I. & Lomas, M. R. Vegetation dynamics—simulating responses to climatic change. *Biol. Rev.* **79,** 643–670 (2004).
71. Zaehle, S. & Friend, A. D. Carbon and nitrogen cycle dynamics in the O-CN land surface model I: model description, site-scale evaluation, and sensitivity to parameter estimates. *Glob. Biogeochem. Cycles* **24,** GB1005 (2010).
72. Krinner, G. *et al*. A dynamic global vegetation model for studies of the coupled atmosphere-biosphere system. *Glob. Biogeochem. Cycles* **19,** GB1015 (2005).
73. Oleson, K. *et al*. Improvements to the Community Land Model and their impact on the hydrological cycle. *J. Geophys. Res.* **113,** G01021 (2008).
74. Exbrayat, J. F., Pitman, A. J., Zhang, Q., Abramowitz, G. & Wang, Y. P. Examining soil carbon uncertainty in a global model: response of microbial decomposition to temperature, moisture and nutrient limitation. *Biogeosciences* **10,** 7095–7108 (2013).
75. Hengl, T. *et al*. SoilGrids1km—global soil information based on automated mapping. *PLoS ONE* **9,** e105992 (2014).
76. Sen, P. K. Estimates of the regression coefficient based on Kendall's tau. *J. Am. Stat. Assoc.* **63,** 1379–1389 (1968).
77. Jones, P., Parker, D., Osborn, T. & Briffa, K. *Trends: A Compendium of Data on Global Change* 1–5 (Oak Ridge National Laboratory, Carbon Dioxide Information Analysis Center, 2006).
78. Karl, T. R. *et al*. Possible artifacts of data biases in the recent global surface warming hiatus. *Science* **348,** 1469–1472 (2015).
79. Trenberth, K. E. Has there been a hiatus? *Science* **349,** 691–692 (2015).
80. Li, W. *et al*. Reducing uncertainties in decadal variability of the global carbon budget with multiple datasets. *Proc. Natl Acad. Sci. USA* **113,** 13104–13108 (2016).